inorganics

Article

Oxygen Ion and Proton Transport in Alkali-Earth Doped Layered Perovskites Based on $BaLa_2In_2O_7$

Nataliia Tarasova [1,2,*], Anzhelika Bedarkova [1,2], Irina Animitsa [1,2], Ksenia Belova [1,2], Ekaterina Abakumova [1,2], Polina Cheremisina [1,2] and Dmitry Medvedev [1,2]

1 Institute of High Temperature Electrochemistry of the Ural Branch of the Russian Academy of Sciences, Akademicheskaya St., 620066 Yekaterinburg, Russia
2 Institute of Hydrogen Energy, Ural Federal University, Mira St. 19, 620075 Yekaterinburg, Russia
* Correspondence: Natalia.Tarasova@urfu.ru

Abstract: Inorganic materials with layered perovskite structures have a wide range of physical and chemical properties. Layered perovskites based on $BaLa_nIn_nO_{3n+1}$ ($n = 1, 2$) were recently investigated as protonic conductors. This work focused on the oxygen ion and proton transport (ionic conductivity and mobility) in alkali-earth (Sr^{2+}, Ba^{2+})-doped layered perovskites based on $BaLa_2In_2O_7$. It is shown that in the dry air conditions, the nature of conductivity is mixed oxygen–hole, despite the dopant nature. Doping leads to the increase in the conductivity values by up to ~1.5 orders of magnitude. The most proton-conductive $BaLa_{1.7}Ba_{0.3}In_2O_{6.85}$ and $BaLa_{1.7}Sr_{0.15}In_2O_{6.925}$ samples are characterized by the conductivity values $1.2{\cdot}10^{-4}$ S/cm and $0.7{\cdot}10^{-4}$ S/cm at 500 °C under wet air, respectively. The layered perovskites with Ruddlesden-Popper structure, containing two layers of perovskite blocks, are the prospective proton-conducting materials and further material science searches among this class of materials is relevant.

Keywords: layered perovskite; Ruddlesden-Popper structure; oxygen ion conductivity; proton conductivity

Citation: Tarasova, N.; Bedarkova, A.; Animitsa, I.; Belova, K.; Abakumova, E.; Cheremisina, P.; Medvedev, D. Oxygen Ion and Proton Transport in Alkali-Earth Doped Layered Perovskites Based on $BaLa_2In_2O_7$. *Inorganics* **2022**, *10*, 161. https://doi.org/10.3390/inorganics10100161

Academic Editor: Antonino Gulino

Received: 14 September 2022
Accepted: 29 September 2022
Published: 1 October 2022

1. Introduction

The layered perovskite family includes such classes of perovskite-related structures as Ruddlesden-Popper (RP), Dion–Jacobson (DJ), and Aurivillius structures (Figure 1). Compounds with a Ruddlesden-Popper structure have the general formula $A_{n+1}B_nO_{3n+1}$, in which the rock salt layers AO alternate with perovskite blocks $(ABO_3)_n$. This type of structure was described for the first time for the compositions Sr_2TiO_4 [1] and $Sr_2Ti_2O_7$ [2] by S.N. Ruddlesden and P. Popper in 1957–1958. Aurivillius phases are characterized by the formula $A_{n-1}Bi_2B_nO_{3n+3}$, which describes alternation of perovskite layers $A_{n-1}B_nO_{3n+1}$ with layers of a fluorite structure, formed by bismuth and oxygen ions $[Bi_2O_2]^{2+}$. This crystal structure was first described in 1949 by B. Aurivillius [3]. Dion–Jacobson phases can be described by the formula $A'A_{n-1}B_nO_{3n+1}$. The structure of these compounds includes perovskite blocks $A_{n-1}B_nO_{3n+1}$ separated by layers, in which only metal cations A′ are presented. The mixed niobates of alkali and alkaline earth metals with such type of structure were synthesized for the first time by M. Dion [4] and A.J. Jacobson [5,6] in the first half of the 1980s.

The materials with layered perovskite-related structures have many various applications due to their different physical–chemical properties. They are known as photocatalysts [7–13], and include materials for solar hydrogen production [14–17], ferroelectrics [18–22], and phosphors [22–28]. Some of RP and DJ materials are capable of water molecule intercalation into the interlayer space. Ion exchange leads to the formation of protonated forms of compositions, for example $H_xLn_{1-x}TiO_4{\cdot}nH_2O$ [29–32] or $H_{1-x}La_xCa_{2-x}Nb_3O_{10}$ [33,34]. Recently, the possibility of dissociative incorporation of water molecules into crystal lattice was proven for the RP compositions based on $AA'BO_4$ (A = Ba, Sr, A′ = La, Nd, B = In, Sc) and $AA'_2B_2O_7$ (A = Ba, A′ = La, Nd, B = In). The materials based on the monolayer perovskites $BaNdInO_4$ [35–40], $BaLaScO_4$ [41], $SrLaInO_4$ [42–46], and $BaLaInO_4$ [47–52] were investigated as protonic conductors in the temperature range of 300–500 °C. It is shown that doping of the cationic sublattices is a successful way to improve the oxygen ion and proton transport [53]. Two-layer perovskites $BaLa_2In_2O_7$ [54] and $BaNd_2In_2O_7$ [55] are also investigated as proton conductors. The acceptor doping of the lanthanum sublattice of $BaLa_2In_2O_7$ allows for an increase in the ionic conductivity of the matrix composition [56]. In this work, the effect of acceptor dopant (Sr^{2+}, Ba^{2+}) concentration on the ionic transport (O^{2-}, H^+) of $BaLa_{2-x}M_xIn_2O_{7-0.5x}$ solid solutions, including the effect on the oxygen and proton mobility, was found.

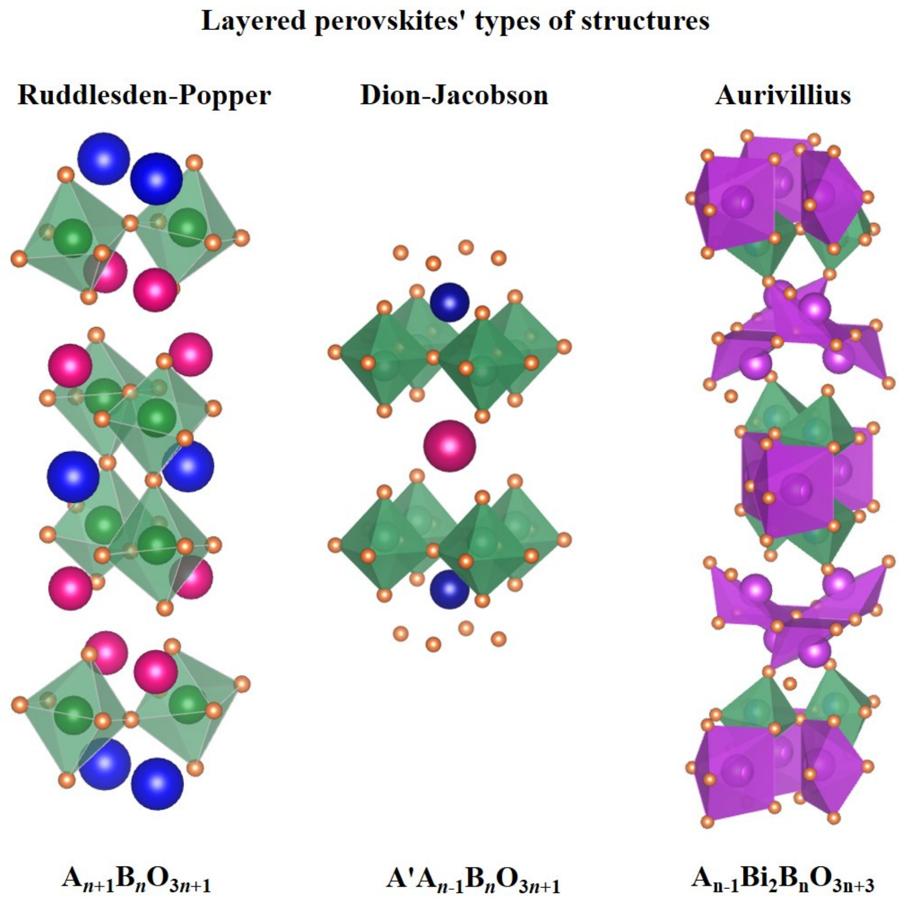

Figure 1. The images of layered perovskites types of structures: Ruddlesden-Popper ($A_{n+1}B_nO_{3n+1}$), Dion–Jacobson ($A'A_{n-1}B_nO_{3n+1}$), and Aurivillius ($A_{n-1}Bi_2B_nO_{3n+3}$) (from left to right) with $n = 2$.

2. Results and Discussion

2.1. XRD and TG Investigations

The X-ray diffraction (XRD) analysis was applied to establish the homogeneity ranges of the solid solutions $BaLa_{2-x}M_xIn_2O_{7-0.5x}$ (M = Sr, Ba). The single-phase compositions were obtained in the ranges $0 \leq x \leq 0.20$ and $0 \leq x \leq 0.30$ for the Sr- and Ba-doped solid solutions, respectively (tetragonal symmetry, *P4₂/mnm* space group). The introduction of ions with bigger ionic radius ($r_{La^{3+}}$ = 1.216 Å, $r_{Sr^{2+}}$ = 1.31 Å, $r_{Ba^{2+}}$ = 1.47 Å [57]) leads to the increase in the lattice parameters and unit cell volumes of doped compositions (Tables 1 and 2). Figure 2a represents the example of a full-profile analysis for the $BaLa_{1.8}Ba_{0.2}In_2O_{6.9}$ composition.

Table 1. Lattice parameters, unit cell volume, and water uptake for $BaLa_{2-x}Sr_xIn_2O_{7-0.5x}$.

Sample	a, b (Å)	c (Å)	Vcell (Å^3)	Water Uptake (mol)
0	5.914(9)	20.846(5)	729.3365	0.17
0.05	5.915(2)	20.869(0)	730.1977	0.15
0.10	5.916(3)	20.870(4)	730.5183	0.18
0.15	5.916(4)	20.871(3)	730.5745	0.18
0.20	5.917(2)	20.872(1)	730.8001	0.19

Table 2. Lattice parameters, unit cell volume, and water uptake for $BaLa_{2-x}Ba_xIn_2O_{7-0.5x}$.

Sample	a, b (Å)	c (Å)	Vcell (Å^3)	Water Uptake (mol)
0	5.914(9)	20.846(5)	729.3365	0.17
0.05	5.915(1)	20.859(0)	729.8232	0.16
0.10	5.916(3)	20.870(4)	730.5183	0.17
0.15	5.920(4)	20.899(3)	732.5442	0.19
0.20	5.927(5)	20.940(1)	735.7357	0.20
0.25	5.941(5)	20.949(1)	739.5330	0.21
0.30	5.956(6)	20.954(9)	743.5025	0.22

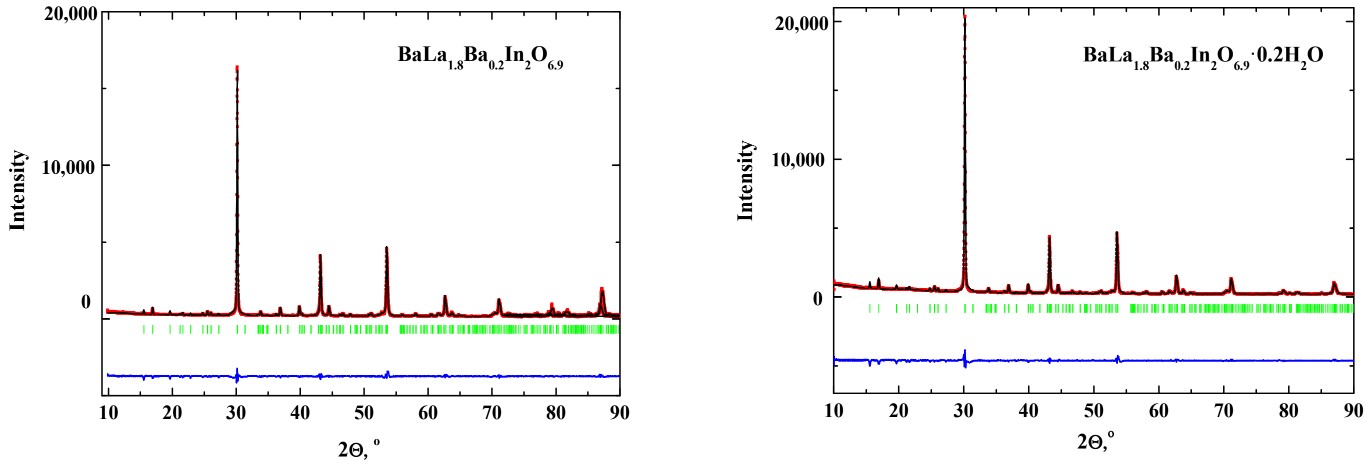

(**a**) (**b**)

Figure 2. The XRD data for the anhydrous $BaLa_{1.8}Ba_{0.2}In_2O_{6.9}$ (**a**) and hydrated $BaLa_{1.8}Ba_{0.2}In_2O_{6.9}\cdot 0.2H_2O$ (**b**) compositions.

The possibility for water uptake was investigated by the thermogravimetry (TG) method. The amounts of water uptake for each composition are presented in the Tables 1 and 2. As can be seen, water uptake for all undoped and doped compositions is close, and it is in the range 0.15–0.22 mol water per formula unit. It should be added that these values are comparable with water uptake for acceptor-doped classic perovskites. The TG curve coupled with MS water signal for the hydrated composition $BaLa_{1.8}Ba_{0.2}In_2O_{6.9}\cdot 0.2H_2O$ are presented in Figure 3.

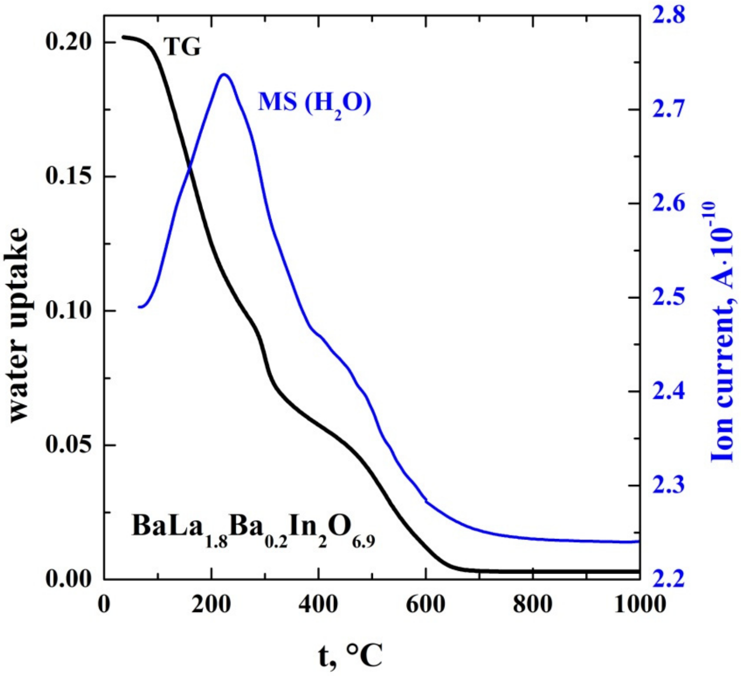

Figure 3. The TG and MS(H_2O) curves of $BaLa_{1.8}Ba_{0.2}In_2O_{6.9}\cdot 0.2H_2O$ composition.

The dissociative incorporation of water for the classic perovskites $ABO_{3-\delta}$ is due to the interaction of oxygen vacancies $V_o^{\bullet\bullet}$ (appearing by the acceptor doping) or $V_o^{\times}$ (own structural defects) with water molecules:

$$V_o^{\bullet\bullet} + H_2O + O_o^{\times} \Leftrightarrow 2(OH)_o^{\bullet}, \quad (1)$$

$$V_o^{\times} + H_2O + 2O_o^{\times} \Leftrightarrow 2(OH)_o^{\bullet} + O_i'', \quad (2)$$

where $V_o^{\bullet\bullet}$ is the oxygen vacancy, $O_o^{\times}$ is the oxygen atom in the regular position, $(OH)_o^{\bullet}$ is the hydroxyl group in the oxygen sublattice, and O_i'' is the oxygen atom in the interstitial position.

Accordingly, the amount of water uptake must increase with increase in the oxygen vacancy concentration in the crystal structure of a doped complex oxide:

$$2MO \overset{La_2O_3}{\rightarrow} 2M_{La}' + 2O_o^{\times} + V_o^{\bullet\bullet}, \quad (3)$$

where M_{La}':Sr or Ba atoms in La sites; $V_o^{\bullet\bullet}$: oxygen vacancy; and $O_o^{\times}$: oxygen atom in a regular position. However, the water uptake for the monolayer perovskites based on $BaLaInO_4$ is much bigger than oxygen vacancy concentration, and it depends on the space size between perovskite blocks in the structure [53]. In this case, the dissociative intercalation of water can be described as the incorporation of hydroxyl groups into space between perovskite blocks:

$$H_2O + O_o^{\times} \Leftrightarrow (OH)_o^{\bullet} + (OH)_i', \quad (4)$$

where $(OH)_o^{\bullet}$ is the hydroxyl group in the regular oxygen position and $(OH)_i'$ is the hydroxyl group located in the rock salt block. It is also shown that the water uptake for the two-layer $BaLa_2In_2O_7$ composition is lower compared to the monolayer $BaLaInO_4$ composition (0.17 vs. 0.62 mol per formula unit, respectively) [55]. In other words, monolayer and two-layer barium–lanthanum indates have different hydration relationships. The obtained results concerning water uptake for $BaLa_{1-x}M_xIn_2O_{7-x}$ (M = Sr, Ba) also prove this. Obviously, the presence in the structure of two octahedral layers of perovskite blocks means less structural flexibility of the crystal lattice during hydration, and this factor is more significant than the increase in the lattice parameter and oxygen vacancies concentration during doping. In contrast to the previously described hydrated solid solutions based on $BaLaInO_4 \cdot nH_2O$, the investigated hydrated solid solutions based on $BaLa_{2-x}M_xIn_2O_{7-0.5x} \cdot nH_2O$ do not change the symmetry; these solid solutions are described by the same *P4₂/mnm* space group as anhydrous $BaLa_{2-x}M_xIn_2O_{7-0.5x}$ (M = Sr, Ba) phases also (Figure 2b).

2.2. Electrical Conductivity Investigations

The general view of the temperature dependencies of conductivities is the same for the all investigated compositions of $BaLa_{2-x}M_xIn_2O_{7-0.5x}$ (M = Sr, Ba). As an example, the temperature dependencies of conductivity obtained under different oxygen and water partial pressure are presented in Figure 4 for the composition $BaLa_{1.75}Ba_{0.25}In_2O_{6.875}$.

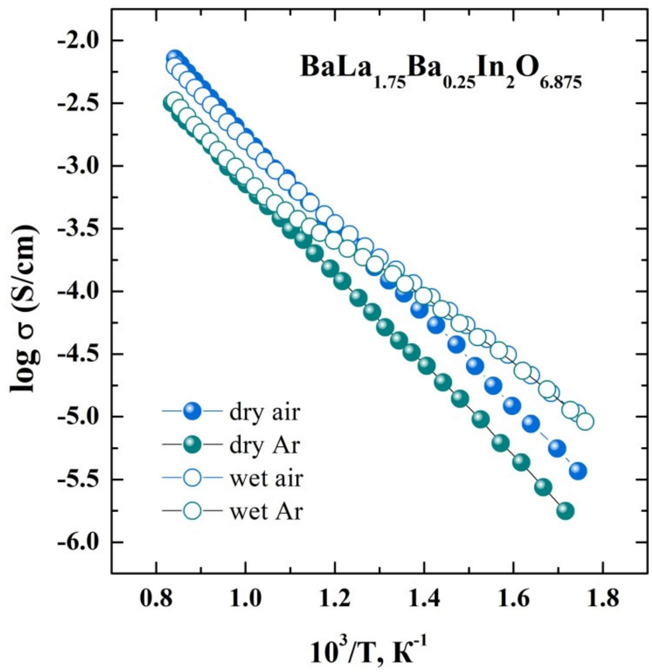

Figure 4. The temperature dependencies of conductivity for the composition $BaLa_{1.75}Ba_{0.25}In_2O_{6.875}$ under dry (filled symbols) and wet (open symbols) conditions.

As can be seen, the values obtained under low pO_2 (~10^{-5} atm, Ar) and low pH_2O ($3.5 \cdot 10^{-5}$ atm, dry atmosphere) conditions are lower than under dry air (pO_2 = 0.21 atm, $pH_2O = 3.5 \cdot 10^{-5}$ atm) conditions. The difference is about 0.5 order of magnitude over the whole investigated temperature range. The effect of high water partial pressure ($pH_2O = 2 \cdot 10^{-2}$ atm, wet atmosphere) on the conductivity values is more significant at the temperatures below ~500 °C. In this temperature region (300–500 °C), conductivity values under wet conditions are higher that under dry conditions by about 0.4 order of magnitude under air and 0.8 order under Ar. In addition, the conductivity values under wet air and wet Ar are very close at T < 500 °C. Figure 5 represents the concentration dependencies of conductivities for both solid solutions $BaLa_{2-x}M_xIn_2O_{7-0.5x}$ (M = Sr, Ba) at 500 °C under dry air. As can be seen, the maximum for the concentration dependencies of conductivities is observed for both solid solutions. The difference in the conductivity values under different oxygen partial pressure (air and Ar) indicates the mixed ionic–electronic nature of electrical conductivity (Figure 4). Consequently, the detailed analysis of the dependence of conductivity on oxygen partial pressure is necessary.

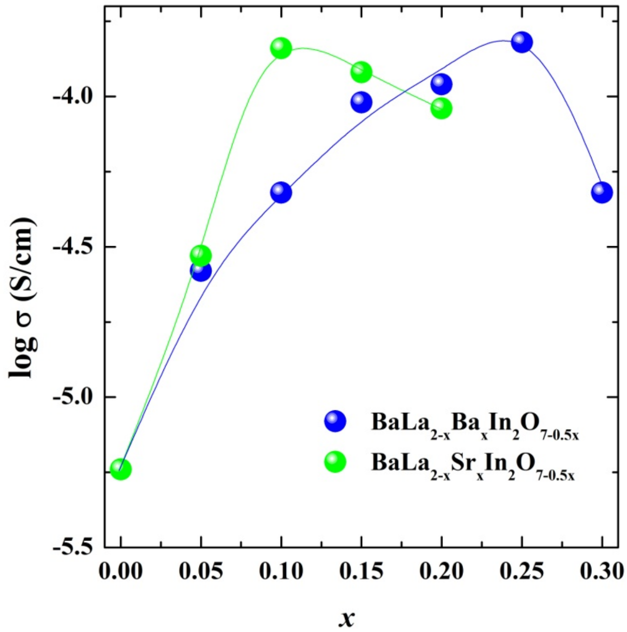

Figure 5. The concentration dependencies of electrical conductivity at 500 °C under dry air for the solid solutions $BaLa_{2-x}M_xIn_2O_{7-0.5x}$ (M = Sr, Ba).

The σ−pO_2 dependencies obtained under dry and wet conditions for the doped compositions are presented in Figure 6. All dependencies for Sr and Ba compositions have the same regularities, which are discussed below. It should be noted that the shape of σ−pO_2 dependencies for undoped and doped compositions are also similar [54].

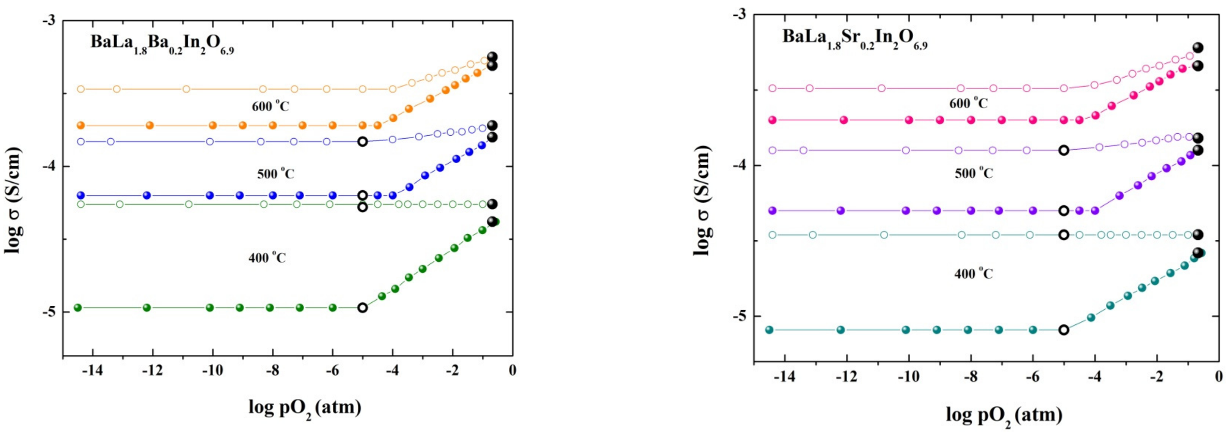

(**a**) (**b**)

Figure 6. The dependencies of the conductivity values vs. oxygen partial pressure for the compositions $BaLa_{1.8}Ba_{0.2}In_2O_{6.9}$ (**a**) and $BaLa_{1.8}Sr_{0.2}In_2O_{6.9}$ (**b**) under dry (filled symbols) and wet (open symbols) conditions and conductivity values from σ–10^3/T dependencies under wet air (filled black symbols) and wet Ar (open black symbols) conditions.

Under dry air and oxidizing conditions ($pO_2 > 10^{-4}$ atm), the nature of conductivity is mixed ionic–hole, and the process of the appearance of holes can be written by the following equation:

$$V_o^{\bullet\bullet} + 1/2O_2 \Leftrightarrow O_o^{\times} + 2h^{\bullet}, \quad (5)$$

where $V_o^{\bullet\bullet}$ is the oxygen vacancy, $O_o^{\times}$ is the oxygen atom in the regular position, and $h^{\bullet}$ is the hole. The area of predominant oxygen ionic conductivity is observed at $pO_{2,}$ lower than 10^{-4} atm. The conductivity values obtained under the Ar atmosphere are localized in the electrolytic region (black open symbols in Figure 6), which allows us to consider the values obtained in dry argon as oxygen ion conductivity values.

The concentration dependencies of oxygen ion conductivity obtained at different temperatures are presented in Figure 7. As can be seen, these dependencies exhibit a similar shape to the dependencies of total (mixed ionic–electronic) conductivities (Figure 5). The maxima on the curves are recorded for the Sr-doped composition at x = 0.1 and for Ba-doped compositions at x = 0.15–0.25. In the other words, doping by both Sr^{2+} and Ba^{2+} ions leads to an increase in the oxygen ionic conductivity values. The possible reasons are the increase in the oxygen vacancies concentration and the expansion of space for ionic transport (increase in the lattice parameters and unit cell volumes) during doping. At the same time, the conductivity decreases in the area of high dopant concentrations. The most possible cause may be an association of point defects and the formation of the clusters:

$$\mathrm{M}'_{\mathrm{La}} + \mathrm{V}_{\mathrm{o}}^{\bullet\bullet} \rightarrow \left(\mathrm{M}'_{\mathrm{La}} \cdot \mathrm{V}_{\mathrm{o}}^{\bullet\bullet}\right)^{\bullet} \text{ or} \tag{6}$$

$$\mathrm{M}'_{\mathrm{La}} + \left(\mathrm{M}'_{\mathrm{La}} \cdot \mathrm{V}_{\mathrm{o}}^{\bullet\bullet}\right)^{\bullet} \rightarrow \left(2\mathrm{M}'_{\mathrm{La}} \cdot \mathrm{V}_{\mathrm{o}}^{\bullet\bullet}\right)^{\times}, \tag{7}$$

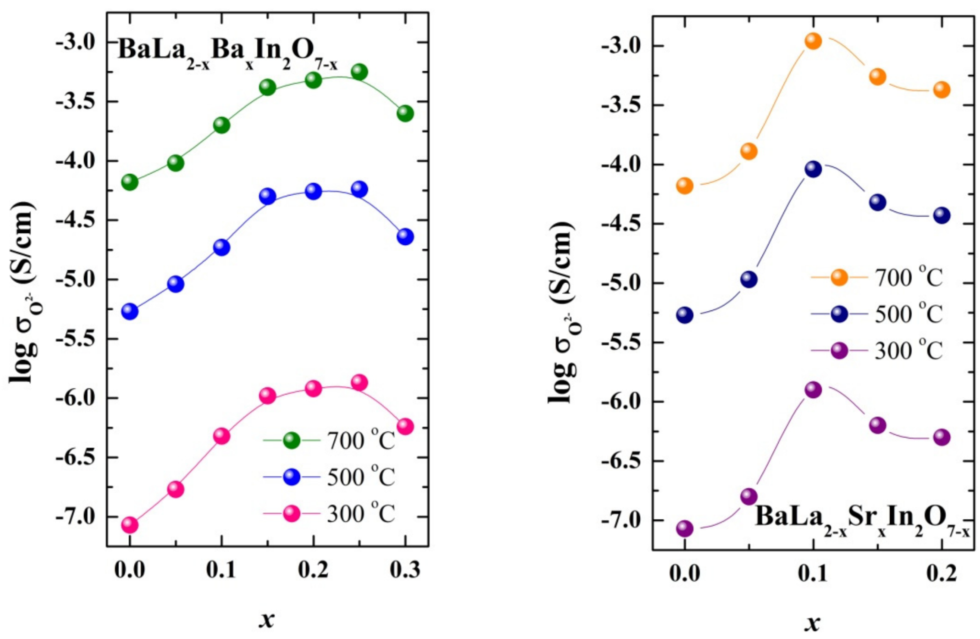

(**a**) (**b**)

Figure 7. The concentration dependencies of oxygen ion conductivity at 300, 500, and 700 °C for the solid solutions $BaLa_{2-x}Ba_xIn_2O_{7-0.5x}$ (**a**) and $BaLa_{2-x}Sr_xIn_2O_{7-0.5x}$ (**b**).

The observed decrease in the oxygen vacancy mobility at the high dopant concentrations (Figure 8) proves this assumption. It should be noted that the similar effect of decreasing the oxygen ion conductivity and mobility is observed for the Ba-doped solid solution based on monolayer $BaLaInO_4$ composition [47].

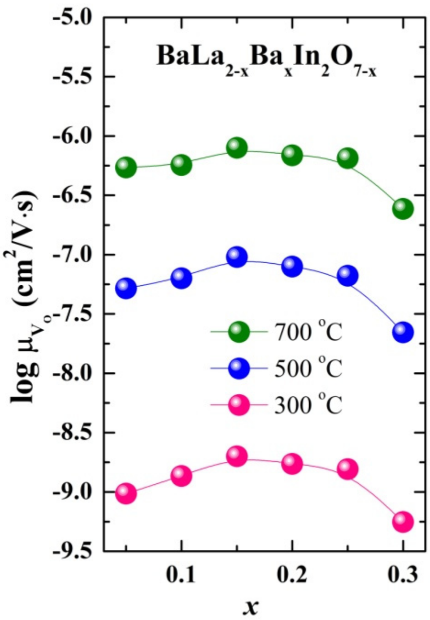

(**a**)

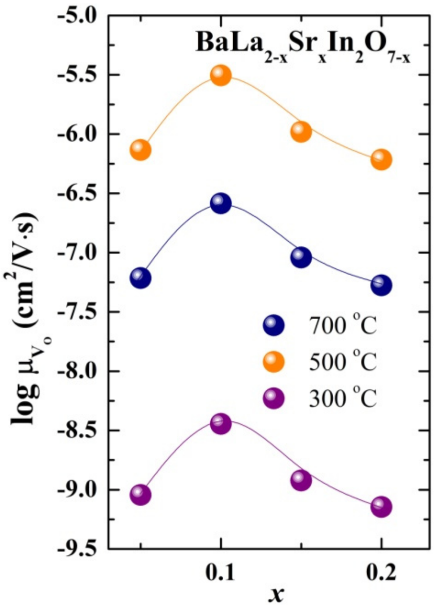

(**b**)

Figure 8. The concentration dependencies of oxygen ions mobility at 700, 500, and 300 °C for the solid solutions $BaLa_{2-x}Ba_xIn_2O_{7-0.5x}$ (**a**) and $BaLa_{2-x}Sr_xIn_2O_{7-0.5x}$ (**b**).

The interaction of water molecules with the crystal lattice of layered perovskites based on $BaLa_2In_2O_7$ can be expressed by Equation (4) or by the following reaction:

$$BaLa_2In_2O_7 + \frac{x}{2}H_2O \Leftrightarrow BaLa_2In_2O_{7+\frac{x}{2}}(OH)_x. \quad (8)$$

Consequently, the hydrated forms of complex oxides can be written, for example, as $BaLa_2In_2O_{6.83}(OH)_{0.34}$ (undoped composition). The effect of the water partial pressure on conductivity is more pronounced in the electrolytic region (Figure 6). The increase in the proton concentration during decreasing temperature leads to the decrease in the hole concentration and, consequently, in the hole conductivity:

$$h^{\bullet} + 1/2H_2O + O_o^{\times} \Leftrightarrow 1/4O_2 + (OH)_o^{\bullet}. \quad (9)$$

The predominance of protonic transport is achieved below ~450 °C. The good comparability between conductivity values obtained under wet Ar (black open signs in Figure 6) and values obtained from σ–pO_2 dependencies at $pO_2 = 10^{-5}$ atm should be noted.

Proton conductivity values were calculated as the difference between the conductivity values in wet and dry Ar, and its concentration dependencies for the solid solutions $BaLa_{2-x}M_xIn_2O_{7-0.5x}$ are presented in Figure 9. As can be seen, the proton conductivity increases with increasing dopant concentration. However, the most significant increase is observed in the area of "small" dopant concentrations ($x \leq 0.10$ for Sr-doped and $x \leq 0.15$ s for Ba-doped solid solutions). The further increase in the dopant concentration leads to the small increase in conductivity (Ba-doped solid solution) or results in no effect (Sr-doped solid solution).

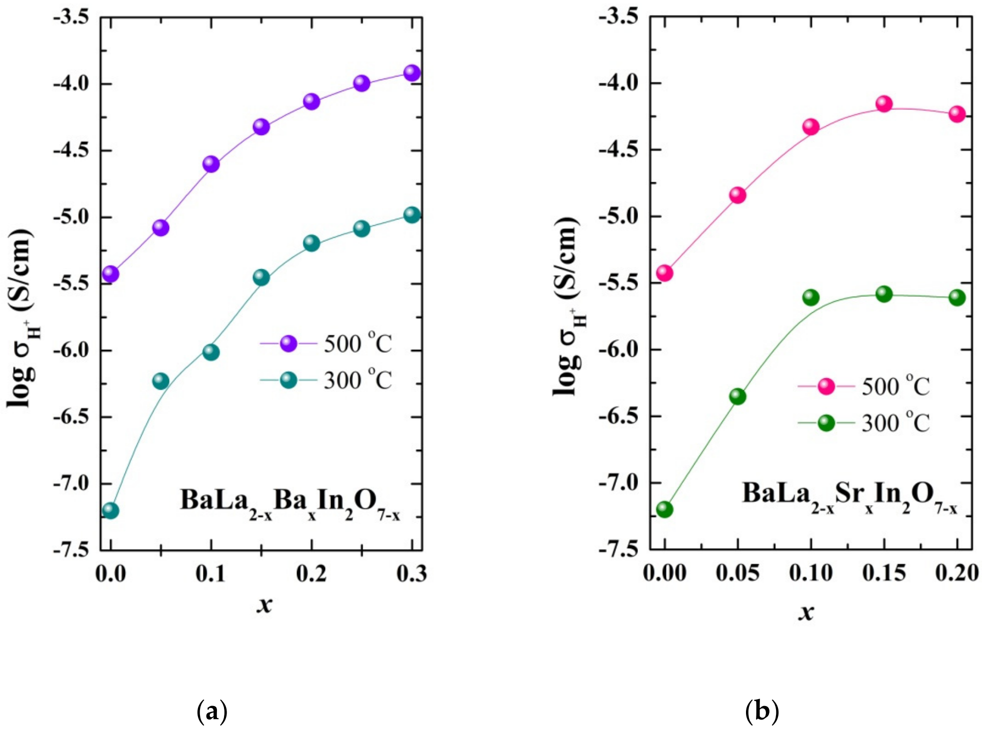

Figure 9. The concentration dependencies of proton conductivity at 500 and 300 °C for the solid solutions $BaLa_{2-x}Ba_xIn_2O_{7-0.5x}$ (**a**) and $BaLa_{2-x}Sr_xIn_2O_{7-0.5x}$ (**b**).

The concentration dependencies of proton mobilities at 300 °C are presented in Figure 10. As can be seen, the increase in the proton mobility is observed in the area of "small" dopant concentration, and it can be associated with the increase in the oxygen ion mobility in this area (Figure 8). The further increase in the dopant concentration leads to the decrease in the proton concentration (Sr-doped solid solution) or to an insufficient increase (Ba-doped solid solution). Obviously, the cluster formation occurs in the wet atmosphere also:

$$M'_{La} + (OH)^{\bullet}_{o} \rightarrow (M'_{La} \cdot (OH)^{\bullet}_{o})^{\times}, \quad (10)$$

and this process is more significant for the compositions with smaller dopant size M'_{La} (that is, for the Sr-doped compositions). It should be noted that the same effect of decreasing the proton mobility under "high" dopant concentrations is observed for the Ba-doped solid solution based on the monolayer $BaLaInO_4$ composition [47].

Thus, the acceptor doping of two-layer perovskite $BaLa_2In_2O_7$ is a successful way for improving proton conductivity and obtaining novel high-conductive electrolytic materials. The doping by the Sr^{2+}- and Ba^{2+}- ions on the La^{3+} sublattice leads to the increase in the ion conductivity by up to ~1.5 orders of magnitude. The most proton-conductive compositions $BaLa_{1.7}Ba_{0.3}In_2O_{6.85}$ and $BaLa_{1.7}Sr_{0.15}In_2O_{6.925}$ have close conductivity values of 1.2×10^{-4} S/cm and 0.7×10^{-4} S/cm at 500 °C under wet air, respectively.

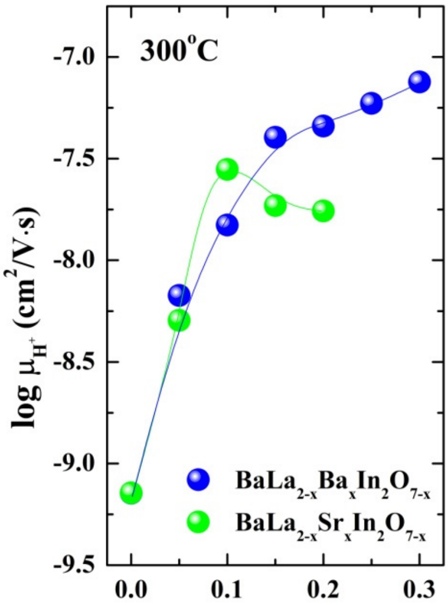

Figure 10. The concentration dependencies of oxygen ions mobility at 300 °C for the solid solutions $BaLa_{2-x}Ba_xIn_2O_{7-0.5x}$ and $BaLa_{2-x}Sr_xIn_2O_{7-0.5x}$.

3. Materials and Methods

Two-layer perovskites $BaLa_{2-x}M_xIn_2O_{7-0.5x}$ (M = Sr, Ba) were prepared by the solid-state method. The carbonates $BaCO_3$ and $SrCO_3$, and oxides In_2O_3 and In_2O_3 (99.99% purity, REACHIM, Moscow, Russia) were initially dried, then weighed (analytical balance (Sartorius AG, Göttingen, Germany)) and mixed in stoichiometric quantities. The agate mortar was used for milling the powders. The calcination was performed at 800, 900, 1000, 1100, 1200, and 1300 °C. The time of each temperature treatment was 24 h.

The X-ray analysis was performed using a Bruker Advance D8 Cu K_α diffractometer (Bruker, Billerica, MA, USA) with step of 0.01°, scanning rate of 0.5°/min.

The thermogravimetry (TG) and mass spectrometry (MS) analysis were performed using STA 409 PC Netzsch Analyser connected with QMS 403 C Aëolos mass spectrometer (Netzsch, Selb, Germany). The heating of initially hydrated samples was conducted in the temperature range of 40–1100 °C, with the rate of 10 °C/min under a flow of dry Ar.

The measurements of electrical conductivity were performed by impedance spectroscopy method (impedance spectrometer Z-1000P, (Electrochemical Instruments (Elins), Chernogolovka, Russia). The investigations were conducted from 1000 to 200 °C with 1°/min cooling rate under dry air or dry Ar conditions. The dry gas (air or Ar) was produced by circulating the gas through P_2O_5 ($pH_2O = 3.5 \cdot 10^{-5}$ atm). The wet gas (air or Ar) was obtained by bubbling the gas at room temperature first through distilled water, and then through saturated solution of KBr ($pH_2O = 2 \cdot 10^{-2}$ atm). The humidity of the gas was controlled by a Honeywell HIH-3610 H_2O sensor (Honeywell, Freeport, TX, USA). The dependencies of conductivities vs. partial oxygen pressures pO_2 were obtained by using the electrochemical method for producing different pO_2 with oxygen pump from Y-stabilized ZrO_2 ceramic. The values of the resistance were recorded after 3–5 h of equilibrium.

4. Conclusions

It this paper, the members of the layered perovskites family with a two-layer Ruddlesden-Popper structure were obtained, and theirs transport properties were investigated. It is shown that doping of the lanthanum sublattice of $BaLa_2In_2O_7$ by the ions Sr^{2+} and Ba^{2+} with bigger ionic radius leads to the increase in lattice parameters and unit cell volumes of doped compositions. The possibility for dissociative incorporation of water molecules into crystal lattice is proven. The water uptake is in the range of 0.15–0.22 mol water per formula unit of complex oxide for all undoped and doped compositions. In the dry air conditions, the nature of conductivity is mixed oxygen–hole, regardless of the dopant nature (Sr^{2+}, Ba^{2+}). Doping leads to the increase in the conductivity values by up to ~1.5 orders of magnitude. The most proton-conductive $BaLa_{1.7}Ba_{0.3}In_2O_{6.85}$ and $BaLa_{1.7}Sr_{0.15}In_2O_{6.925}$ samples are characterized by the conductivity values of $1.2 \cdot 10^{-4}$ S/cm and $0.7 \cdot 10^{-4}$ S/cm at 500 °C under wet air, respectively. The acceptor-doped layered perovskites based on $BaLa_2In_2O_7$ are prospective proton-conducting materials, and further material science searches among this class of materials are relevant.

Author Contributions: Conceptualization, N.T. and I.A.; methodology, N.T. and I.A.; investigation, A.B., K.B., P.C. and E.A.; data curation, A.B., K.B., P.C. and E.A.; writing—original draft preparation, N.T. and I.A.; writing—review and editing, N.T., I.A. and D.M. All authors have read and agreed to the published version of the manuscript.

Funding: This research received no external funding.

Data Availability Statement: Not applicable.

Conflicts of Interest: The authors declare no conflict of interest.

References

1. Ruddlesden, S.N.; Popper, P. New compounds of the K_2NiF_4 type. *Acta Cryst.* **1957**, *10*, 538–539. [CrossRef]
2. Ruddlesden, S.N.; Popper, P. The compound $Sr_3Ti_2O_7$ and its structure. *Acta Cryst.* **1958**, *11*, 54–55. [CrossRef]
3. Aurivillius, B. Mixed bismuth oxides with layer lattices: I. Structure type of $CaBi_2B_2O_9$.. *Arkiv Kem* **1949**, *1*, 463–480.
4. Dion, M.; Ganne, M.; Tournoux, M. Nouvelles familles de phases $M^IM^{II}{}_2Nb_3O_{10}$ a feuillets «perovskites». *Mater. Res. Bull.* **1981**, *16*, 1429–1435. [CrossRef]
5. Jacobson, A.J.; Lewandowski, J.T.; Johnson, J.W. Ion exchange of the layered perovskite $KCa_2Nb_3O_{10}$ by protons. *J. Less-Common Met.* **1986**, *116*, 137–145. [CrossRef]
6. Jacobson, A.J.; Johnson, J.W.; Lewandowski, J.T. Interlayer chemistry between thick transition-metal oxide layers: Synthesis and intercalation reactions of $K[Ca_2Na_{n-3}Nb_nO_{3n+1}]$. *Inorg. Chem.* **1985**, *24*, 3727–3729. [CrossRef]
7. Domen, K.; Yoshimura, J.; Sekine, T.; Tanaka, A.; Onishi, T. A novel series of photocatalysts with an ion-exchangeable layered structure of niobate. *Catal Lett.* **1990**, *4*, 339–343. [CrossRef]
8. Machida, M.; Yabunaka, J.; Kijima, T. Efficient photocatalytic decomposition of water with the novel layered tantalate $RbNdTa_2O_7$. *Chem. Commun.* **1999**, 1939–1940. [CrossRef]
9. Machida, M.; Miyazaki, K.; Matsushima, S.; Arai, M. Photocatalytic properties of layered perovskite tantalates, $MLnTa_2O_7$ (M = Cs, Rb, Na, and H.; Ln = La, Pr, Nd, and Sm). *J. Mater. Chem.* **2003**, *13*, 1433–1437. [CrossRef]
10. Rodionov, I.A.; Zvereva, I.A. Photocatalytic activity of layered perovskite-like oxides in practically valuable chemical reactions. *Russ. Chem. Rev.* **2016**, *85*, 248–279. [CrossRef]
11. Krasheninnikova, O.V.; Syrov, E.V.; Smirnov, S.M.; Suleimanov, E.V.; Fukina, D.G.; Knyazev, A.V.; Titaev, D.N. Synthesis, crystal structure and photocatalytic activity of new Dion-Jacobson type titanoniobates. *J. Solid State Chem.* **2022**, *315*, 123445. [CrossRef]
12. Phuruangrat, A.; Ekthammathat, N.; Dumrongrojthanath, P.; Thongtem, S.; Thongtem, T. Hydrothermal synthesis, structure, and optical properties of pure and silver-doped Bi_2MoO_6 nanoplates. *Russ. J. Phys. Chem.* **2015**, *89*, 2443–2448. [CrossRef]
13. Chawla, H.; Chandra, A.; Ingole, P.P.; Garg, S. Recent advancements in enhancement of photocatalytic activity using bismuth-based metal oxides Bi_2MO_6 (M = W, Mo, Cr) for environmental remediation and clean energy production. *Ind. Eng. Chem. Res.* **2021**, *95*, 1–15. [CrossRef]
14. Tasleem, S.; Tahir, M. Recent progress in structural development and band engineering of perovskites materials for photocatalytic solar hydrogen production: A review. *Int. J. Hydrogen Energy* **2020**, *45*, 19078–19111. [CrossRef]
15. Huang, Y.; Liu, J.; Deng, Y.; Qian, Y.; Jia, X.; Ma, M.; Yang, C.; Liu, K.; Wang, Z.; Qu, S.; et al. The application of perovskite materials in solar water splitting. *J. Semicond.* **2020**, *41*, 011701. [CrossRef]
16. Zhang, G.; Liu, G.; Wang, L.; Irvine, J.T.S. Inorganic perovskite photocatalysts for solar energy utilization. *Chem. Soc. Rev.* **2016**, *45*, 5951–5984. [CrossRef] [PubMed]
17. Zhang, P.; Zhang, J.; Gong, J. Tantalum-based semiconductors for solar water splitting. *Chem. Soc. Rev.* **2014**, *43*, 4395–4422. [CrossRef]
18. Benedek, N.A.; Rondinelli, J.M.; Djani, H.; Ghosez, P.; Lightfoot, P. Understanding ferroelectricity in layered perovskites: New ideas and insights from theory and experiments. *Dalton Trans.* **2015**, *44*, 10543–10558. [CrossRef]
19. Ferreira, W.C.; Rodrigues, G.L.C.; Araújo, B.S.; de Aguiar, F.A.A.; de Abreu Silva, A.N.A.; Fechine, P.B.A.; de Araujo Paschoal, C.W.; Ayala, A.P. Pressure-induced structural phase transitions in the multiferroic four-layer Aurivillius ceramic $Bi_5FeTi_3O_{15}$. *Ceram. Int.* **2020**, *46*, 18056–180621. [CrossRef]
20. Zulhadjri; Wendari, T.P.; Ikhram, M.; Putri, Y.E.; Septiani, U.; Imelda. Enhanced dielectric and ferroelectric responses in La^{3+}/Ti^{4+} co-substituted $SrBi_2Ta_2O_9$ Aurivillius phase. *Ceram. Int.* **2022**, *48*, 10328–103321. [CrossRef]

21. Xu, Q.; Xie, S.; Wang, F.; Liu, J.; Shi, J.; Xing, J.; Chen, Q.; Zhu, J.; Wang, Q. Bismuth titanate based piezoceramics: Structural evolutions and electrical behaviors at different sintering temperatures. *J. Alloys Compd.* **2021**, *882*, 160637. [CrossRef]
22. Chen, C.; Ning, H.; Lepadatu, S.; Cain, M.; Yan, H.; Reece, M.J. Ferroelectricity in Dion-Jacobson $ABiNb_2O_7$ (A = Rb, Cs) compounds. *J. Mater. Chem. C* **2015**, *3*, 19–22. [CrossRef]
23. Kudo, A.; Kaneko, E. Photoluminescence of layered perovskite oxides with triple-octahedra slabs containing titanium and niobium. *J. Mater. Sci. Lett.* **1997**, *16*, 224–226. [CrossRef]
24. Pavani, K.; Graça, M.P.F.; Kumar, J.S.; Neves, A.J. Photoluminescence varied by selective excitation in $BiGdWO_6$:Eu^{3+} phosphor. *Opt. Mater.* **2017**, *74*, 120–127. [CrossRef]
25. Mamidi, S.; Gundeboina, R.; Kurra, S.; Velchuri, R.; Muga, V. Aurivillius family of layered perovskites, $BiREWO_6$ (RE = La, Pr, Gd, and Dy): Synthesis, characterization, and photocatalytic studies. *Comptes Rendus Chim.* **2018**, *21*, 547–552. [CrossRef]
26. Zhou, G.; Jiang, X.; Zhao, J.; Molokeev, M.; Lin, Z.; Liu, Q.; Xia, Z. Two-dimensional-layered perovskite $ALaTa_2O_7$:Bi^{3+} (A = K and Na) phosphors with versatile structures and tunable photoluminescence. *ACS Appl. Mater. Interfaces* **2018**, *10*, 24648–24655. [CrossRef]
27. Panda, D.P.; Singh, A.K.; Kundu, T.K.; Sundaresan, A. Visible-light excited polar Dion-Jacobson $Rb(Bi_{1-x}Eu_x)_2Ti_2NbO_{10}$ perovskites: Photoluminescence properties and in vitro bioimaging. *J. Mater. Chem. B* **2022**, *10*, 935–944. [CrossRef]
28. Yadav, D.; Nirala, G.; Kumar, U.; Upadhyay, S. Investigation on structural and optical properties of system $Sr_2Ce_{1-x}Na_xO_4$ ($0.0 \leq x \leq 0.10$). *J. Mater. Sci. Mater. Electron.* **2021**, *32*, 8064–8080. [CrossRef]
29. Schaak, E.R.; Mallouk, T.E. $KLnTiO_4$ (Ln = La, Nd, Sm, Eu, Gd, Dy): A new series of Ruddlesden-Popper phases synthesized by ion-exchange of $HLnTiO_4$. *J. Solid State Chem.* **2001**, *161*, 225–232. [CrossRef]
30. Nishimoto, S.; Matsuda, M.; Miyake, M. Novel protonated and hydrated n = 1 Ruddlesden-Popper phases, $H_xNa_{1-x}LaTiO_{4-y}H_2O$, formed by ion-exchange/intercalation reaction. *J. Solid State Chem.* **2005**, *178*, 811–818. [CrossRef]
31. Nishimoto, S.; Matsuda, M.; Harjo, S.; Hoshikawa, A.; Kamiyama, T.; Ishigaki, T.; Miyake, M. Structural change in a series of protonated layered perovskite compounds, $HLnTiO_4$ (Ln = La, Nd and Y). *J. Solid State Chem.* **2006**, *179*, 1892–1897. [CrossRef]
32. Kurnosenko, S.A.; Silyukov, O.I.; Mazur, A.S.; Zvereva, I.A. Synthesis and thermal stability of new inorganic-organic perovskite-like hybrids based on layered titanates $HLnTiO_4$ (Ln = La, Nd). *Ceram. Int.* **2020**, *46*, 5058–5068. [CrossRef]
33. Huang, Y.; Xie, Y.; Fan, L.; Li, Y.; Wei, Y.; Lin, J.; Wu, J. Synthesis and photochemical properties of La-doped $HCa_2Nb_3O_{10}$. *Int. J. Hydrogen Energy* **2008**, *33*, 6432–6438. [CrossRef]
34. Zhou, C.; Shi, R.; Waterhouse, G.I.N.; Zhang, T. Recent advances in niobium-based semiconductors for solar hydrogen production. *Coord. Chem. Rev.* **2020**, *419*, 213399. [CrossRef]
35. Fujii, K.; Esaki, Y.; Omoto, K.; Yashima, M.; Hoshikawa, A.; Ishigaki, T.; Hester, J.R. New perovskite-related structure family of oxide-ion conducting materials $NdBaInO_4$. *Chem. Mater.* **2014**, *26*, 2488–2491. [CrossRef]
36. Fujii, K.; Shiraiwa, M.; Esaki, Y.; Yashima, M.; Kim, S.J.; Lee, S. Improved oxide-ion conductivity of $NdBaInO_4$ by Sr doping. *J. Mater. Chem. A* **2015**, *3*, 11985. [CrossRef]
37. Ishihara, T.; Yan, Y.; Sakai, T.; Ida, S. Oxide ion conductivity in doped $NdBaInO_4$. *Solid State Ion.* **2016**, *288*, 262–265. [CrossRef]
38. Yang, X.; Liu, S.; Lu, F.; Xu, J.; Kuang, X. Acceptor doping and oxygen vacancy migration in layered perovskite $NdBa_{1-n}O_4$-based mixed conductors. *J. Phys. Chem. C* **2016**, *120*, 6416–6426. [CrossRef]
39. Fijii, K.; Yashima, M. Discovery and development of $BaNdInO_4$ -A brief review. *J. Ceram. Soc. Jpn.* **2018**, *126*, 852–859. [CrossRef]
40. Zhou, Y.; Shiraiwa, M.; Nagao, M.; Fujii, K.; Tanaka, I.; Yashima, M.; Baque, L.; Basbus, J.F.; Mogni, L.V.; Skinner, S.J. Protonic conduction in the $BaNdInO_4$ structure achieved by acceptor doping. *Chem. Mater.* **2021**, *33*, 2139–2146. [CrossRef] [PubMed]
41. Shiraiwa, M.; Kido, T.; Fujii, K.; Yashima, M. High-temperature proton conductors based on the (110) layered perovskite $BaNdScO_4$. *J. Mat. Chem. A* **2021**, *9*, 8607. [CrossRef]
42. Kato, S.; Ogasawara, M.; Sugai, M.; Nakata, S. Synthesis and oxide ion conductivity of new layered perovskite $La_{1-x}Sr_{1+x}InO_{4-d}$. *Solid State Ion.* **2002**, *149*, 53–57. [CrossRef]
43. Troncoso, L.; Alonso, J.A.; Aguadero, A. Low activation energies for interstitial oxygen conduction in the layered perovskites $La_{1+x}Sr_{1-x}InO_{4+d}$. *J. Mater. Chem. A* **2015**, *3*, 17797–17803. [CrossRef]
44. Troncoso, L.; Alonso, J.A.; Fernández-Díaz, M.T.; Aguadero, A. Introduction of interstitial oxygen atoms in the layered perovskite $LaSrIn_{1-x}BxO_{4+\delta}$ system (B=Zr, Ti). *Solid State Ion.* **2015**, *282*, 82–87. [CrossRef]
45. Troncoso, L.; Mariño, C.; Arce, M.D.; Alonso, J.A. Dual oxygen defects in layered $La_{1.2}Sr_{0.8-x}Ba_xInO_{4+d}$ (x = 0.2, 0.3) oxide-ion conductors: A neutron diffraction study. *Materials* **2019**, *12*, 1624. [CrossRef] [PubMed]
46. Troncoso, L.; Arce, M.D.; Fernández-Díaz, M.T.; Mogni, L.V.; Alonso, J.A. Water insertion and combined interstitial-vacancy oxygen conduction in the layered perovskites $La_{1.2}Sr_{0.8-x}Ba_xInO_{4+\delta}$. *New J. Chem.* **2019**, *43*, 6087–6094. [CrossRef]
47. Tarasova, N.; Animitsa, I.; Galisheva, A. Electrical properties of new protonic conductors $Ba_{1+x}La_{1-x}InO_{4-0.5x}$ with Ruddlesden-Popper structure. *J. Solid State Electrochem.* **2020**, *24*, 1497–1508. [CrossRef]
48. Tarasova, N.; Galisheva, A.; Animitsa, I. Improvement of oxygen-ionic and protonic conductivity of $BaLaInO_4$ through Ti doping. *Ionics* **2020**, *26*, 5075–5088. [CrossRef]
49. Tarasova, N.; Galisheva, A.; Animitsa, I. Ba^{2+}/Ti^{4+}- co-doped layered perovskite $BaLaInO_4$: The structure and ionic (O^{2-}, H^+) conductivity. *Int. J. Hydrogen Energy* **2021**, *46*, 16868–16877. [CrossRef]
50. Tarasova, N.; Animitsa, I.; Galisheva, A. Effect of acceptor and donor doping on the state of protons in block-layered structures based on $BaLaInO_4$. *Solid State Commun.* **2021**, *323*, 14093. [CrossRef]

51. Tarasova, N.; Galisheva, A.; Animitsa, I.; Anokhina, I.; Gilev, A.; Cheremisina, P. Novel mid-temperature $Y^{3+} \rightarrow In^{3+}$ doped proton conductors based on the layered perovskite $BaLaInO_4$. *Ceram. Int.* **2022**, *48*, 15677–15685. [CrossRef]
52. Tarasova, N.; Animitsa, I.; Galisheva, A.; Korona, D.; Davletbaev, K. Novel proton-conducting layered perovskite based on $BaLaInO_4$ with two different cations in B-sublattice: Synthesis, hydration, ionic (O^{2-}, H^+) conductivity. *Int. J. Hydrogen Energy* **2022**, *47*, 18972–18982. [CrossRef]
53. Tarasova, N.; Animitsa, I. Materials $A^{II}LnInO_4$ with Ruddlesden-Popper structure for electrochemical applications: Relationship between ion (oxygen-ion, proton) conductivity, water uptake and structural changes. *Materials* **2022**, *15*, 114. [CrossRef]
54. Tarasova, N.; Galisheva, A.; Animitsa, I.; Korona, D.; Kreimesh, H.; Fedorova, I. Protonic Transport in layered perovskites $BaLa_nIn_nO_{3n+1}$ (n = 1, 2) with Ruddlesden-Popper Structur. *Appl. Sci.* **2022**, *12*, 4082. [CrossRef]
55. Tarasova, N.; Galisheva, A.; Animitsa, I.; Belova, K.; Egorova, A.; Abakumova, E.; Medvedev, D. Layered perovskites $BaM_2In_2O_7$ (M = La, Nd): From the structure to the ionic (O^{2-}, H^+) conductivity. *Materials* **2022**, *15*, 3488. [CrossRef]
56. Tarasova, N.; Galisheva, A.; Animitsa, I.; Korona, D.; Abakumova, E.; Medvedev, D. Novel mixed oxygen-electronic conductors based on $BaLa_2In_2O_7$ with two-layer Ruddlesden-Popper structure. *Ceram* **2022**, *48*, 35376–35385. [CrossRef]
57. Shannon, R.D. Revised effective ionic radii and systematic studies of interatomic distances in halides and chalcogenides. *Acta Cryst.* **1976**, *A32*, 751–767. [CrossRef]